

1 **Reconnection acceleration in Saturn’s dayside magnetodisc: a multicase study with**
2 **Cassini**

3 R. L. Guo^{1,2}, Z. H. Yao², N. Sergis^{3,10}, Y. Wei^{1,11}, D. Mitchell⁴, E. Roussos⁵, B. Palmaerts²,
4 W. R. Dunn⁶, A. Radioti², L. C. Ray⁷, A. J. Coates⁶, D. Grodent², C. S. Arridge⁷, P.
5 Kollmann⁴, N. Krupp⁵, J. H. Waite⁸, M. K. Dougherty⁹, J. L. Burch⁸, W. X. Wan¹

6

7 1 Key Laboratory of Earth and Planetary Physics, Institute of Geology and Geophysics,
8 Chinese Academy of Sciences, Beijing, China

9 2 Laboratoire de Physique Atmospherique et Planetaire, STAR institute, Universite de
10 Liege, Liege, Belgium

11 3 Office for Space Research and Technology, Academy of Athens, Athens, Greece

12 4 Applied Physics Laboratory, Johns Hopkins University, Laurel, Maryland, USA

13 5 Max-Planck-Institute für Sonnensystemforschung, Göttingen, Germany

14 6 UCL Mullard Space Science Laboratory, Dorking, RH5 6NT, UK

15 7 Department of Physics, Lancaster University, Bailrigg, Lancaster LA1 4YB, UK

16 8 Southwest Research Institute, San Antonio, TX, United States

17 9 Faculty of Natural Sciences, Department of Physics, Imperial College, London, UK

18 10 Institute of Astronomy, Astrophysics, Space Applications and Remote Sensing,
19 National Observatory of Athens, Athens

20 11 College of Earth Sciences, University of Chinese Academy of Sciences, Beijing,
21 China

22

23 **Abstract**

24 Recently, rotationally driven magnetic reconnection was firstly discovered in
25 Saturn’s dayside magnetosphere (Guo et al. 2018). This newly confirmed process
26 could potentially drive bursty phenomena at Saturn, i.e., pulsating energetic particles
27 and auroral emissions. Using Cassini’s measurements of magnetic fields and charged
28 particles, we investigate particle acceleration features during three magnetic
29 reconnection events observed in Saturn’s dayside magnetodisc. The results suggest
30 that the rotationally driven reconnection process plays a key role in producing
31 energetic electrons (up to 100 keV) and ions (several hundreds of keV). In particular,
32 we find that energetic oxygen ions are locally accelerated at all three reconnection
33 sites. Isolated, multiple reconnection sites were recorded in succession during an
34 interval lasting for much less than one Saturn rotation period. Moreover, a secondary
35 magnetic island is reported for the first time at the dayside, collectively suggesting
36 that the reconnection process is not steady and could be ‘drizzle-like’. This study
37 demonstrates the fundamental importance of internally driven magnetic
38 reconnection in accelerating particles in Saturn’s dayside magnetosphere, and
39 likewise in the rapidly rotating Jovian magnetosphere and beyond.

40

41 **Introduction**

42 Magnetic reconnection is a fundamental physical process that converts energy

43 and accelerates charged particles in cosmic, laboratory, and space plasma
44 environments (Zweibel & Yamada 2009). Magnetic reconnection changes the
45 magnetic topology of a system and can couple different plasma populations (Hesse
46 et al. 2017). This process plays a pivotal role in driving the interaction between
47 external interplanetary magnetic fields and internal planetary magnetic fields
48 (Dungey 1961), as well as driving the plasma dynamics inside planetary
49 magnetospheres (e.g., in the nightside planetary magnetotails (Arridge et al. 2016;
50 Hones 1979)).

51 Direct evidence of magnetopause reconnection has been reported at Earth
52 (Paschmann et al. 1979) and other planets such as Mercury (Slavin et al. 2009) and
53 Saturn (McAndrews et al. 2008). In the nightside magnetotail of Earth and Mercury,
54 magnetic reconnection is considered to release the nightside magnetic energy that is
55 accumulated via dayside magnetopause reconnection and plasma circulation.
56 Magnetic reconnection and its consequent production of plasmoids and secondary
57 islands also play important roles on magnetic flux closure in the nightside of Saturn's
58 magnetosphere (Arridge et al. 2016; Jackman et al. 2011).

59 The kronian and jovian magnetospheres are, however, significantly different
60 from the terrestrial and hermean magnetospheres for two major reasons: 1) their
61 magnetospheres rotate much more rapidly, 2) they have internal plasma sources
62 from their rings and moons, which inject hot plasmas into the magnetosphere
63 system. Internally produced plasma in rapidly rotating magnetic environments is
64 radially transported outward (Bagenal et al. 2016), and causes the magnetosphere to
65 attain a stretched magnetic field configuration, termed the magnetodisc. Similar to
66 the terrestrial and hermean magnetospheres, magnetic reconnection at Jupiter and
67 Saturn has also been identified at their magnetopauses and the magnetotails
68 (Arridge et al. 2016; Badman et al. 2013; Huddleston et al. 1997; Masters 2017).
69 Moreover, the magnetic reconnection process on the nightside of the giant planetary
70 magnetospheres can be driven not only by solar wind energy, but also by internal
71 energy, known as internally driven magnetic reconnection (Jackman et al. 2011;
72 Kronberg et al. 2007; Vasylunas 1983). By surveying magnetic measurements from
73 Cassini-MAG instrument, Delamere et al. (2015) revealed that the reconnection
74 indicator (i.e., negative signature of the B_θ magnetic component in Kronographic
75 Radial-Theta-Phi (KRTP) coordinates, a spherical polar coordinates) could exist at all
76 local times, including high probabilities of occurrence at the unexpected pre-noon
77 sectors, and suggested that the reconnection processes were 'drizzle-like' that occur
78 at small patchy regions. Plasma injection into Saturn's inner magnetosphere is also
79 revealed to exist at all local times (Azari et al. 2018). Guo et al. (2018) directly
80 confirmed the existence of magnetic reconnection in Saturn's dayside magnetodisc
81 (i.e., well inside the magnetopause) by examining the reconnection-associated Hall
82 current system and the reconnection acceleration plasma features (including
83 electrons and ions). They showed that heavy ions were accelerated up to 600 keV by
84 the dayside magnetodisc reconnection (DMR). Following the DMR signature, 1-hour

85 pulsating energetic electrons were observed, while it is unclear whether the
86 coexistence of DMR and pulsating energetic electrons is a coincidence or if the two
87 processes are physically connected. The quasi-periodic energetic electron pulsation
88 signatures have been reported in many studies at many local times (Mitchell et al.
89 2009; Palmaerts et al. 2016a; Roussos et al. 2016; Yates et al. 2016), and have been
90 suggested to be relevant to the pulsating auroral emissions (Badman et al. 2015;
91 Palmaerts et al. 2016b).

92 In this study, we identify three DMR events, and investigate the associated
93 energetic particle features by using Cassini's multi-instrument measurements. We
94 report details of energetic oxygen ions and electrons in the reconnection region.
95 Pitch angle features of hot electrons are also analyzed for each reconnection process.

96

97 **Cassini observations of reconnection events**

98 We analyze magnetic field observations from the Cassini-MAG instrument
99 (Dougherty et al. 2004), thermal ion and electron measurements with energy range
100 up to 28 keV (electrons) and 50 keV (ions) from Cassini-CAPS/IMS/ELS (Young et al.
101 2004), and energetic (>18 keV (electrons) and > 27 keV (ions)) particle data from the
102 Low-Energy Magnetospheric Measurements System (LEMMS) and the Ion and
103 Neutral Camera (INCA) of the Magnetosphere Imaging Instrument (MIMI) (Krimigis et
104 al., 2004). Hot electron pitch angle information is available by combining the *in-situ*
105 magnetic field and particle data.

106 Reconnection diffusion region is the key region of the magnetic reconnection
107 domain. However, this region is very small and dynamic, and it is very difficult to
108 explore this with a spacecraft. From a realistic perspective, the negative B_θ signature
109 is usually adopted as a simplified indicator of the magnetic reconnection, which can
110 also effectually expose the reconnection diffusion region. We surveyed the Cassini
111 data that collected from 2005 to 2012, and obtained 139 events that contains
112 negative B_θ signatures inside the magnetosphere at the noon sector from 9 LT (Local
113 Time) to 15 LT, with latitude inside 30 degrees. There are 33 events showing
114 correlations between the negative B_θ signatures and the flux increases of the
115 energetic oxygen ion, which is one of the most important species at Saturn. In this
116 work, we identify 3 reconnection diffusion events from the 33 events, and investigate
117 their Hall magnetic signatures and their ambient plasma features.

118

119 **Event 1: 25 November 2005**

120 Figure 1a shows magnetic field components in Kronographic Radial-Theta-Phi
121 coordinates for 25 November 2005 between 11:40 UT and 13:40 UT. Figure 1b shows
122 the magnetic field components in the X-line coordinate system (Arridge et al. 2016),
123 which is a rectangular coordinate system that removes the bend-back effect of the
124 magnetic field lines in magnetodisc. Figure 1c shows energetic electron differential
125 flux from 18 keV to 832 keV measured by the MIMI-LEMMS instrument. Figure 1d
126 shows the energy spectrogram of omni-directional hot electron flux measured by the

127 CAPS-ELS instrument, and Figures 1e-1g shows pitch angle distribution for electrons
128 within three different energy ranges, i.e., from 50 eV to 500 eV, 500 eV to 3 keV, and
129 3 keV to 28 keV. As shown in Figure 1e-1g, the coverage of pitch angles during the
130 whole period was poor, which is a common situation in Cassini's CAPS-ELS dataset,
131 due to the limited field-of-view of the instrument. Figure 1h shows energetic ion
132 (generally protons) differential flux from 27 keV to 4 MeV from MIMI-LEMMS
133 instrument. Figure 1i shows the energy spectrogram for omnidirectional ion flux
134 from CAPS-IMS instrument. Figure 1j shows the energetic oxygen differential flux
135 from 46 keV to nearly 1 MeV from MIMI-INCA instrument.

136 Following the negative B_θ signature in Figure 1a (or positive B_z component in
137 Figure 1b) at $\sim 12:13$ UT and $\sim 13:10$ UT, two magnetic reconnection sites
138 (highlighted in pink) were detected by Cassini in the pre-noon sector (at 9 LT) at a
139 radial distance of $\sim 21 R_S$ (Saturn's Radius, $1R_S = 60,268$ km) from Saturn's center.
140 Moreover, B_r changes sign when B_z reverses, which is consistent with reconnection-
141 produced Hall magnetic fields (Arridge et al. 2016; Guo et al. 2018). As suggested by
142 the correspondingly small $|B_r|$, the spacecraft was in the outflow part of the
143 reconnection region when the negative B_θ was detected.

144 The electron spectrograms (Figure 1d) in the reconnection regions are featured
145 by higher than the ambient plasma energies. The background region (before the
146 highlighted intervals) where electrons have a wide energy region from 10s of eV to \sim
147 1 keV, while electrons in the reconnection sites are mostly from 100s to a few keV.
148 The pitch angle distributions in Figure 1e-1g showed that the electrons in these
149 reconnection sites are approximately isotropic, but are field-aligned outside the
150 reconnection regions. The isotropic pitch angle distribution of electrons is a typical
151 feature of magnetic reconnection outflow region (e.g., Wang et al. (2016)).

152 The energetic electron flux (in Figure 1c) is enhanced during the two negative B_θ
153 intervals and is also correlated to the magnitude of the B_r component. When $|B_r| >$
154 3 nT, the electron flux in both Figure 1c and 1d minimizes, suggesting that the
155 spacecraft was away from the current sheet center. Before the second highlighted
156 region, the energetic electron flux is also increased when $|B_r|$ decreases, suggesting
157 that the reconnection processes have been proceeding for a while and the
158 accelerated electrons have filled in the current sheet. In addition, as shown in Figure
159 1d, the central energy of the electron flux in the second reconnection site is higher
160 than that in the first one. Moreover, the fluxes of energetic protons (tens of keV
161 to >100 keV, shown in Figure 1h) and energetic oxygen ions (> 200 keV, shown in
162 Figure 1j) are mainly enhanced in the second reconnection site. The enhancement of
163 thermal ions (<10 keV) in the first reconnection site can be clearly seen in the ion
164 spectrogram in Figure 1i. The two reconnection events detected nearby have
165 significantly different accelerating features might suggest that they are two individual
166 reconnection sites, and therefore it is consistent with the "drizzle-like" reconnection
167 picture.

168

169 **Event 2: 15 September 2008**

170 Figure 2 shows the second event occurred on 15 September 2008 between
171 11:00 UT and 16:00 UT, in the near-noon sector (at 11.2 LT) and at a radial distance of
172 $\sim 18 R_S$. The large magnitude of the B_r component was expected since Cassini was at
173 high latitudes, similar to the case in Guo et al. (2018), implying that the spacecraft
174 was in the outer layer of the current sheet. The negative B_θ signature in Figure 2a
175 lasted for more than 2 hours from $\sim 11:43$ UT to $\sim 14:24$ UT and is followed by a
176 bipolar B_θ signature around 14:53 UT.

177 The distinct structure at around 14:53 UT is likely a secondary island
178 (highlighted in pink) inside the long-lasting negative B_θ interval. Additionally, in the
179 X-line coordinates (Figure 2b), the bipolar signature of B_r component is consistent
180 with the Hall magnetic fields. The perpendicular flux of hot electrons is enhanced in
181 the positive B_θ region of the secondary island (Figures 2e and 2f), while it is field-
182 aligned in the rest of the long-lasting negative B_θ region. There is no signature in
183 Figure 2d to show that electrons are substantially accelerated inside the secondary
184 island, suggesting that this secondary island is not contracting. This is because that
185 contracting secondary island would strongly energize electrons (Drake et al. 2006).
186 The energetic oxygen flux (Figure 2j) enhances ahead of the encounter with the
187 secondary island, while the energetic electron flux (Figure 2c) increases after the
188 encounter with the positive B_θ region of the secondary island and keeps a high level
189 outside the secondary island, which might be originated from other nearby
190 secondary reconnection sites that generated the secondary island.

191 Besides the secondary island region, the energetic oxygen flux also enhances at
192 the onset of the long-lasting negative B_θ region (marked by the first arrow in Figure
193 2a) and at the end of the negative B_θ region (marked by the second arrow in Figure
194 2a). After $\sim 15:30$ UT, while the energetic electrons flux increases sharply (marked by
195 the black arrow in Figure 2c), the electron spectrogram in Figure 2d broadens to
196 contain electrons with energy less than 100 eV. The pitch-angle for the broadband
197 electron spectrogram is largely enhanced at perpendicular (Figures 2e and 2f),
198 opposite to the bi-directional feature during the negative B_θ interval. The pitch-angle
199 distributions of this event are different to those of the first event where the electrons
200 showed much isotropic features in the negative B_θ region while bi-directional in the
201 background. In the event of Figure 2, bi-directional electrons are seen also in the
202 negative B_θ region. The difference between the two events might be due to the
203 relative positions between Cassini and the current sheet, as the spacecraft's latitude
204 in the second event was much higher than that in the first event. Hence, Cassini may
205 be detecting the outer edge of the current sheet, which could have different plasma
206 characteristics compared to the current center. It could also be due to aperiodic short
207 time scale dynamics that often dominate locally.

208

209 **Event 3: 15 April 2008**

210 The third reconnection event was also observed in the near-noon sector (at 11.5

211 LT) with a radial distance of $\sim 23 R_S$. Figure 3 is organized in same manner as Figure 1
212 and 2, and shows data from 14 April 2008 21:40 UT to 15 April 2008 01:40 UT. There
213 is a short negative B_θ region (transient 1) around 14 April 2008 23:15 UT (dashed
214 vertical line). After transient 1, the B_θ component shows a significant bipolar
215 signature (transient 2) with oscillations between 14 April 23:47 UT to 15 April 00:33
216 UT (highlighted in pink).

217 In transient 2, the corresponding Hall magnetic field is obvious in Figure 3b
218 where the B_Y component reverses from positive to negative. In Figure 3f, the
219 electrons with energies from 500 eV to 3 keV in this interval are enhanced both in
220 the perpendicular and antiparallel directions (we lack parallel information due to the
221 instrument's limited field of view), suggesting that this could be the electron exhaust
222 region, which is the inner part of the reconnection region and is filled by energized
223 electrons that have been accelerated by both the X-line and a parallel potential near
224 the separatrix region (e.g., Egedal et al. (2012) and Wang et al. (2016)).

225 The energetic electron flux in Figure 3c is enhanced when B_θ attained large
226 positive values during transient 2. The energetic oxygen flux increases on both sides
227 of the B_θ bipolar interval and drops at the same time that the energetic electrons are
228 suddenly enhanced. Considering that the electron diffusion region is much smaller
229 than and is surrounded by the oxygen diffusion region, the features of energised
230 plasma can suggest that the spacecraft moved from the oxygen diffusion region on
231 the outer part of the reconnection region (the first oxygen flux enhancement during
232 the transient 2), to the electron exhaust further inside the reconnection region (the
233 oxygen flux decrease and meanwhile electron flux enhancement during the transient
234 2), and then back to the oxygen diffusion region (the second Oxygen flux
235 enhancement during the transient 2).

236 In transient 1, the B_ϕ component was nearly zero before B_θ becomes negative,
237 suggesting the azimuthal bend-back configuration of the magnetodisc (Vasyliunas
238 1983) is mostly eliminated by the reconnection process in this region. Revealed by
239 the plasma properties, the reconnection signatures observed at transient 1 can be
240 divided into three regions, which are indicated above Figure 3d with three horizontal
241 arrows.

242 The first region is where the energetic oxygen and proton fluxes were enhanced,
243 in Figures 3j and 3h, respectively. The electron spectrogram (Figure 3d) shows a
244 cavity in the low energy range. Electrons with energy around 1 keV display a bi-
245 directional pitch angle distribution (Figure 3f), but they are more isotropic above 3
246 keV (Figure 3g). The second region is after the cold electron cavity and before the
247 peak of B_θ component. The energetic electron flux in Figure 3c was sharply enhances
248 in this region. The electron spectrogram has two bands. The low energy band is
249 associated with bi-directional features (Figure 3e), and the high-energy band is
250 roughly isotropic (Figure 3f). The third region is where the B_θ component sharply
251 drops to negative. The electron spectrogram here is again bimodal. The flux of low
252 energy electron band is enhanced in the perpendicular direction (Figure 3e).

253 The double electron bands in transient 1 are likely the mixture of reconnection
254 accelerated population and ambient population. Enhancements in the low energy
255 electron band are correlated with the dips in B_r . The four groups of colored arrows
256 above Figures 3a and 3d show the correspondence between the B_r dips and
257 intensifications in the low energy electron bands. This correlation strongly indicates
258 that the low energy electron population could only exist in the inner current sheet,
259 while high energy electron population could reach to distances farther from the
260 current sheet center (Sergis et al. 2011). The electron population in this event
261 appeared to have different characteristics compared to the other two events
262 presented in this work. A further statistical study of the electron properties at
263 different radial distances, local times and latitudes is required to systematically
264 understand the variable behavior of electrons in different events.

265

266 **Discussion and conclusion**

267 As suggested by Delamere et al. (2015), magnetic reconnection can be expected
268 to occur at any local time and not only in the midnight sector. The unambiguous ion
269 diffusion region reported by Guo et al. (2018) and the three reconnection cases in
270 this study, provide additional and direct evidence of the existence of the dayside
271 magnetodisc reconnection processes, which locally produce energetic electrons and
272 ions with energies of 100s of keV at the dayside magnetosphere.

273 Figure 4 shows the line plots and the energy spectrograms for the flux of
274 energetic hydrogen (top two panels) and oxygen (bottom two panels) during the
275 enhancement in the first event studied here (the second highlighted region in Figure
276 1). The flux peaks across all the energies of the hydrogens and oxygens ions at the
277 same time, eliminating the possibility that our signatures were generated by an
278 injection event and suggesting that the ions were locally accelerated. The
279 spectrograms is similar to that reported in Angelopoulos et al. (2008) for a terrestrial
280 magnetotail reconnection event. It is readily expected that the flux would enhance
281 (drop) when moving towards (away from) the reconnection region, since the
282 magnetic reconnection domain is the source region of energetic particles.

283 Observational features from the three events support the concept of ‘drizzle-like’
284 reconnection process, i.e. reconnection on global scales facilitated through
285 numerous, small-scale reconnection channels (Delamere et al. 2015). For the event
286 on November 25, 2005 (Figure 1), the energy of the hot electrons in the second
287 reconnection site is higher than the first one (Figure 1d). Furthermore, the >10 keV
288 energetic ions prominently appear in the second reconnection site, while it was
289 much quiet in the first one (Figures 1h and 1j). These difference between the
290 accelerated particles suggests that the two detected reconnection signatures are not
291 from the same reconnection site, indicating that Cassini sampled adjacent but
292 independent reconnection channels, a signature consistent with the ‘drizzle’ concept
293 that suggested by Delamere et al. (2015). In addition, the separation of the two
294 reconnection sites in the azimuthal direction was $\sim 12 R_s$, if considering that they co-

295 rotate with the magnetosphere (Yao et al. 2017) in the duration over one hour (the
296 time gap of the two reconnection events). The large separation between the two
297 reconnection regions may exclude the possibility that they come from different
298 evolution stages of the same event. For the event on 15 September 2008 (Figure 2),
299 there is a long-lasting negative B_θ interval. However, because of the lack of the
300 information on the magnetic structure near the current sheet center, it is hard to
301 determine whether the aforementioned negative B_θ signature is caused by one or
302 more reconnection sites. The B_Y signatures are not consistent with the Hall magnetic
303 field signatures outside the negative B_θ regions. This could either be due to the
304 disturbed current sheet, that can result in the X-line coordinates failing to adequately
305 represent the magnetic geometry near the reconnection region, which is very
306 possible near the current sheet center where the magnetic strength is small; or be
307 due to the interference from the nearby reconnection site if the reconnection
308 process was ‘drizzle-like’.

309 The three events show very diverse forms of plasma acceleration, which is
310 naturally expected due to the temporal variations and differences along the Cassini
311 trajectories in crossing the complex magnetic reconnection sites in giant planetary
312 magnetospheres. The presence of oxygen ions throughout the magnetosphere
313 introduces an additional layer to the reconnection site, forming an oxygen diffusion
314 region outside the proton diffusion region. This added layer makes the ion diffusion
315 region enlarged and more complex, as particles exhibit different behavior across
316 diffusion regions. For instance, the energetic oxygen ions concentrate in a narrow
317 angular range within the 90 x 120 degree field-of-view of MIMI-INCA and peak at the
318 pitch angles neither parallel nor perpendicular, while protons present more isotropic
319 features (not shown, informed from MIMI-INCA). The non-gyrotropic and anisotropic
320 feature of the oxygen ions may be due to their non-frozen-in behavior during the
321 acceleration in the diffusion region for their larger gyro-radii (Sergis et al. 2013)
322 comparing to the protons. The efficient perpendicular acceleration on heavy ions has
323 been revealed by Galileo in Jovian magnetotail reconnection region (Radioti et al.
324 2007). Combining with reconnection's parallel acceleration, it is therefore possible to
325 have accelerated energetic heavy ions at a pitch angle between parallel and
326 perpendicular as observed in our events. Additionally, the existence of the secondary
327 island in the second event, suggests the reconnection process is not steady, which
328 will increase the diversity in particle behavior. The reason for the double bands in the
329 electron spectrogram in Figure 3d and their variation might be very complex as the
330 reconnection can couple different populations (Hesse et al. 2017). We expect this
331 coupling to be more pronounced for ‘drizzle’ reconnection, where multiple plasma
332 populations can be mixed on small spatial scales over a broad magnetospheric region.

333 In summary, we detailed characteristics of plasma acceleration for three
334 magnetic reconnection events located in the dayside magnetodisc of Saturn. The
335 heavy ions have strong influence on the evolution of the magnetic reconnection
336 (Liang et al. 2017). Since the content of heavy ions are fundamentally different in

337 giant planets and Earth (Blanc et al. 2015), we would expect a different role of the
338 heavy ions in triggering reconnection process at Saturn and the Earth's
339 magnetospheres. Unsteady and 'drizzle-like' DMR processes at Saturn can energize
340 particles and provide an energy source for exciting auroral emissions connected to
341 Saturn's dayside polar region. Furthermore, if these processes are common and more
342 energetic in Jupiter's magnetosphere, they may offer a crucial means for energizing
343 the heavy ions that precipitate into Jupiter's atmosphere, generating X-ray and UV
344 auroral flares.

345

346 **Acknowledgement:**

347 The work was supported by the National Science Foundation of China (41704169,
348 41525016, 41474155, 41274167). Z. Y., D. G. and B. P. acknowledge financial support
349 from the Belgian Federal Science Policy Office (BELSPO) via the PRODEX Programme
350 of ESA. L.C.R. was funded by an STFC Consolidated Grant to Lancaster University
351 (ST/R000816/1). Cassini operations are supported by NASA (managed by the Jet
352 Propulsion Laboratory) and ESA. The data presented in this paper are available from
353 the NASA Planetary Data System <http://pds-ppi.igpp.ucla.edu/>.

354

355 **References:**

- 356 Angelopoulos, V., et al. 2008, *Science*, 321, 931
357 Arridge, C. S., et al. 2016, *Nature Physics*, 268
358 Azari, A. R., et al. 2018, *Journal of Geophysical Research: Space Physics*, 123, 4692
359 Badman, S. V., et al. 2015, *Space Science Reviews*, 187, 99
360 Badman, S. V., et al. 2013, *Geophysical Research Letters*, 40, 1027
361 Bagenal, F., Wilson, R. J., Siler, S., Paterson, W. R., & Kurth, W. S. 2016, *Journal of*
362 *Geophysical Research: Planets*
363 Blanc, M., et al. 2015, *Space Science Reviews*, 192, 237
364 Delamere, P., Otto, A., Ma, X., Bagenal, F., & Wilson, R. 2015, *Journal of Geophysical*
365 *Research: Space Physics*, 120, 4229
366 Dougherty, M. K., et al. 2004, *Space Science Reviews*, 114, 331
367 Drake, J., Swisdak, M., Che, H., & Shay, M. 2006, *Nature*, 443, 553
368 Dungey, J. W. 1961, *Physical Review Letters*, 6, 47
369 Egedal, J., Daughton, W., & Le, A. 2012, *Nature Physics*, 8, 321
370 Guo, R., et al. 2018, *Nature Astronomy*, 2, 640
371 Hesse, M., Chen, L., Liu, Y.-H., Bessho, N., & Burch, J. 2017, *Physical review letters*,
372 118, 145101
373 Hones, E. W. 1979, *Space Science Reviews*, 23, 393
374 Huddleston, D. E., Russell, C. T., Le, G., & Szabo, A. 1997, *Journal of Geophysical*
375 *Research: Space Physics*, 102, 24289
376 Jackman, C., Slavin, J., & Cowley, S. 2011, *Journal of Geophysical Research: Space*
377 *Physics*, 116, A10212
378 Kronberg, E., Glassmeier, K. H., Woch, J., Krupp, N., Lagg, A., & Dougherty, M. 2007,

379 Journal of Geophysical Research: Space Physics, 112
380 Liang, H., Lapenta, G., Walker, R. J., Schriver, D., El-Alaoui, M., & Berchem, J. 2017,
381 Journal of Geophysical Research: Space Physics, 122, 618
382 Masters, A. 2017, Journal of Geophysical Research: Space Physics, 122, 11
383 McAndrews, H., Owen, C., Thomsen, M., Lavraud, B., Coates, A., Dougherty, M., &
384 Young, D. 2008, Journal of Geophysical Research: Space Physics, 113, A04210
385 Mitchell, D., et al. 2009, Planetary and Space Science, 57, 1732
386 Palmaerts, B., Radioti, A., Roussos, E., Grodent, D., Gérard, J. C., Krupp, N., &
387 Mitchell, D. G. 2016b, Journal of Geophysical Research: Space Physics, 121, 11
388 Palmaerts, B., Roussos, E., Krupp, N., Kurth, W. S., Mitchell, D. G., & Yates, J. N.
389 2016a, Icarus, 271, 1
390 Paschmann, G., et al. 1979, Nature, 282, 243
391 Radioti, A., Woch, J., Kronberg, E. A., Krupp, N., Lagg, A., Glassmeier, K.-H., &
392 Dougherty, M. K. 2007, Journal of Geophysical Research: Space Physics, 112,
393 A06221
394 Roussos, E., et al. 2016, Icarus, 263, 101
395 Sergis, N., et al. 2011, Journal of Geophysical Research: Space Physics, 116
396 Sergis, N., et al. 2013, Journal of Geophysical Research: Space Physics, 118, 1620
397 Slavin, J. A., et al. 2009, science, 324, 606
398 Vasyliunas, V. 1983, Physics of the Jovian magnetosphere, 1, 395
399 Wang, S., Chen, L. J., Bessho, N., Kistler, L. M., Shuster, J. R., & Guo, R. 2016, Journal
400 of Geophysical Research: Space Physics, 121, 2104
401 Yao, Z., et al. 2017, The Astrophysical Journal Letters, 846, L25
402 Yates, J. N., et al. 2016, Geophysical Research Letters, 43, 11
403 Young, D., et al. 2004, Space Science Reviews, 114, 1
404 Zweibel, E. G., & Yamada, M. 2009, Annual review of astronomy and astrophysics,
405 47, 291
406
407

408

409 Figure 1. Dayside magnetodisc reconnection event on 25 November 2005. (a) Three
410 magnetic field components in KRTP coordinates (B_r in blue, B_θ in green and B_ϕ in
411 red), and (b) in reconnection coordinates (B_x in blue, B_y in green and B_z in red). (c)
412 Energetic electron differential flux from MIMI-LEMMS. (d) Energy spectrogram of
413 omni-directional electron flux from CAPS-ELS. (e-g) Pitch angle distribution for
414 electrons within energy ranges of from 50 eV to 500 eV, 500 eV to 3 keV, and 3 keV to
415 28 keV. (h) Energetic proton differential flux from MIMI-LEMMS. (i) Energy
416 spectrogram for omni-directional ion flux from CAPS-IMS. (j) Energetic oxygen
417 differential flux from MIMI-INCA. The pink regions highlighted the two reconnection
418 regions that are identified by combining the signatures of negative B_θ component,
419 Hall magnetic field, and the heated electrons.

420

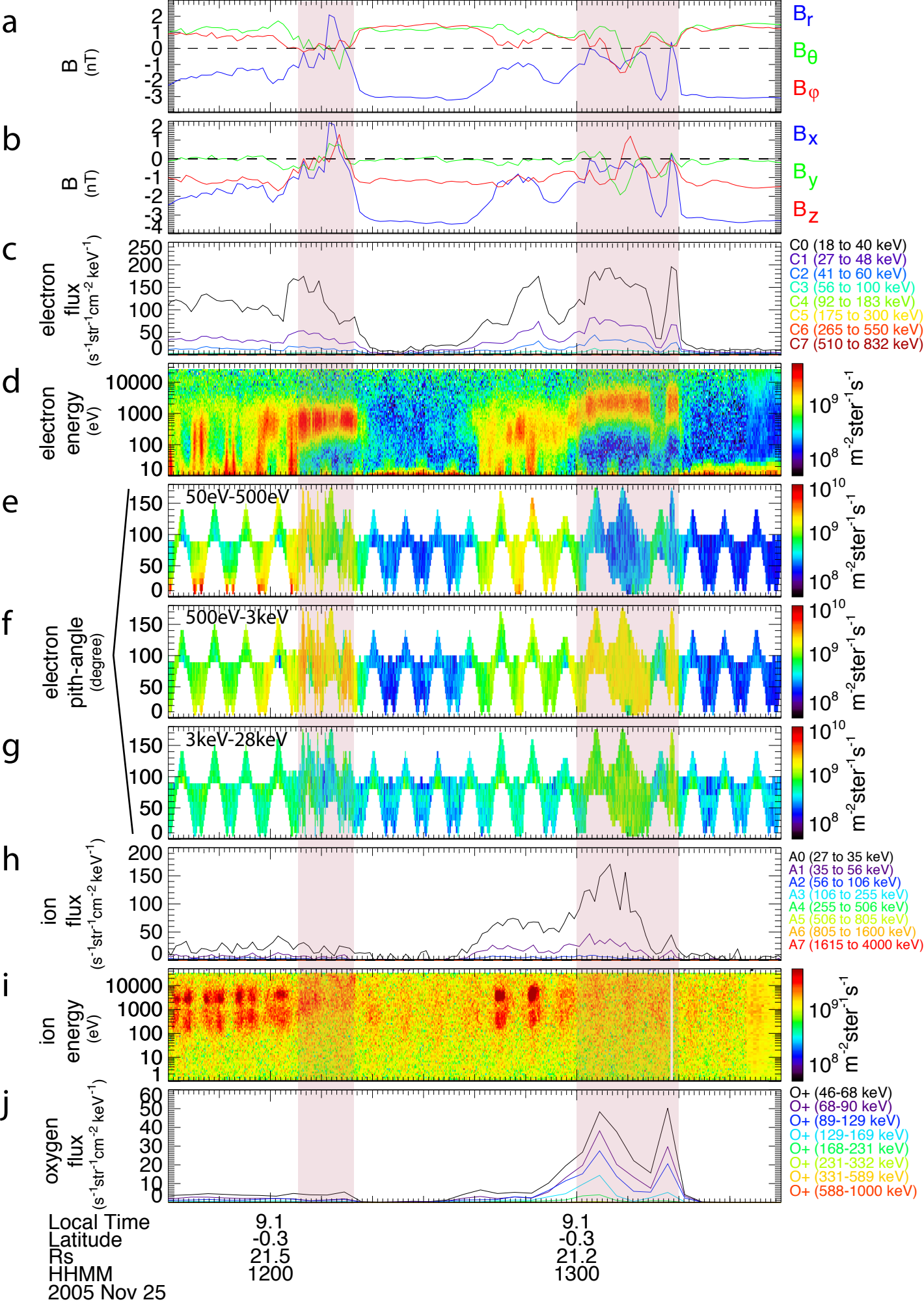
421 Figure 2. Dayside magnetodisc reconnection event on 15 September 2008. The
422 panels are arranged as the same format as Figure 1. The high electron/ion fluxes
423 from C0/A0 channel at the beginning of Figure 2c/2h are due to light contamination.

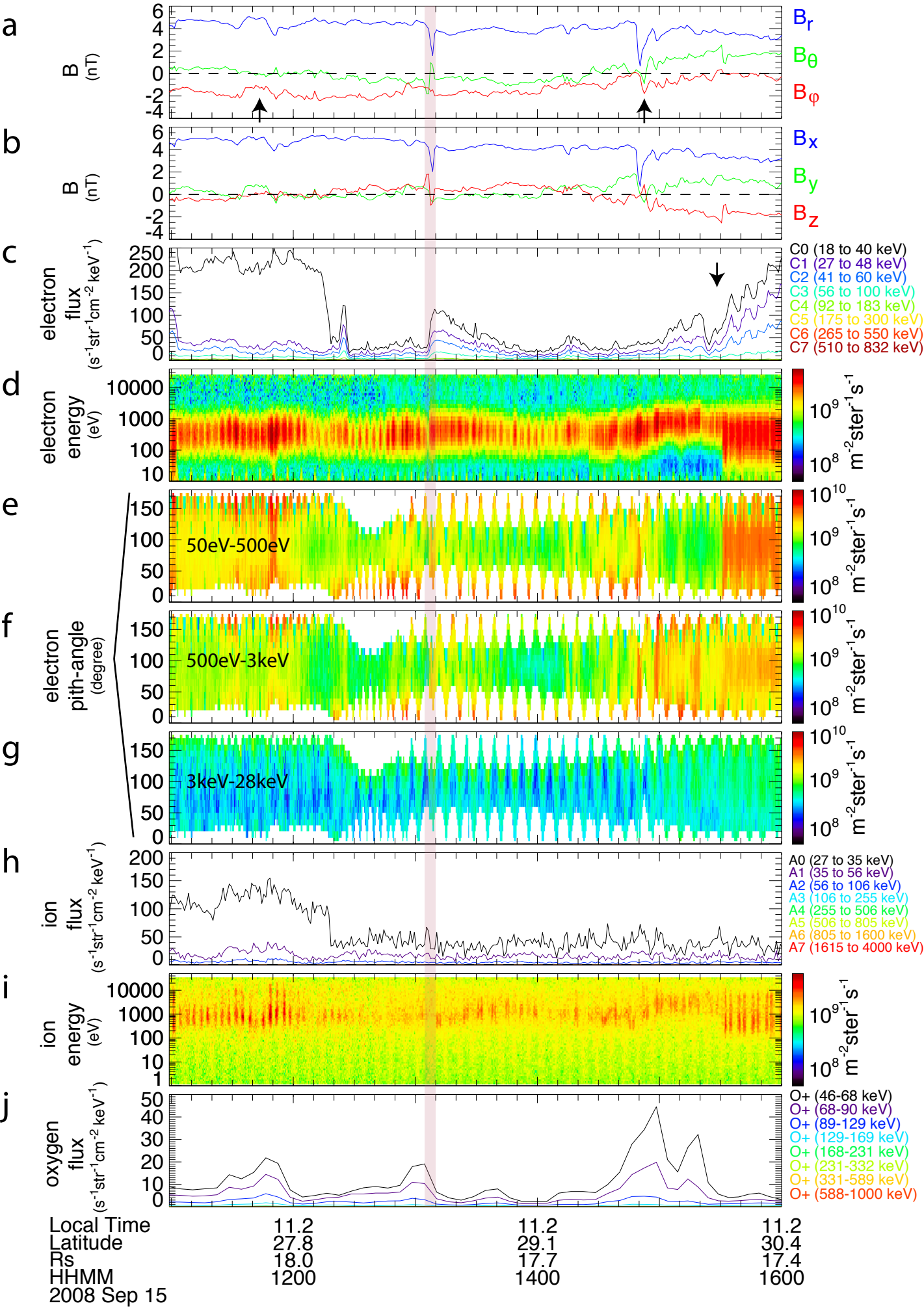
424

425 Figure 3. Dayside magnetodisc reconnection event on April 14th and April 15th in
426 2008. The panels are arranged as the same format as Figure 1 and Figure 2. The four
427 coloured arrows show the correspondence between the B_r dips and the low energy
428 electron bands.

429

430 Figure 4. Differential flux and energy spectrogram for the energetic protons (a-b) and
431 energetic oxygen (c-d) from MIMI-INCA on November 25, 2005, i.e., the first event.
432 There are two major peaks for both protons and oxygen. The fluxes across all
433 energies are enhanced at 13:04 and 13:18 simultaneously.





Transient 1 Transient 2

